Climate Dynamics (2000) 16:63–77

A. Schmittner · C. Appenzeller · T. F. Stocker

Validation of parametrisations for the meridional energy and moisture transport used in simple climate models

Received: 30 November 1998 / Accepted: 4 July 1999

Abstract Parametrisations of meridional energy and moisture transport used in zonally averaged climate models are validated using reanalysis data and results from a doubling CO_2-experiment from a general circulation model. Global meridional fluxes of moisture and sensible heat are calculated by integrating surface and top-of-the-atmosphere vertical fluxes from one pole to the other. The parametrisations include an eddy-diffusion term, representing down-gradient transport of specific humidity and temperature due to the transient atmospheric eddies at mid- and high latitudes, and simple representations of the mean meridional circulation. Qualitative and quantitative agreement between the increased hydrological cycle in the $2 \times CO_2$-run from the GCM and the parametrisation is found. The performance for the sensible heat flux shows larger differences to the GCM results, particularly at low latitudes. Seasonal variations of the moisture and sensible heat transport are well captured by parametrisations including the influence of the mean meridional circulation. Interannual variability cannot be simulated. An examination of the parametrisations on different spatial scales suggests that they should not be used for small scales. Furthermore, two closures for the zonal distribution of precipitation were examined. They are used in zonally averaged atmosphere models coupled to an ocean model with different ocean basins at one latitudinal belt. An assessment of both the reanalysis data and the GCM results shows that both closures exhibit very similar behaviour and are valid in the long-term mean and seasonal cycle. Interannual variability is not captured well. They become invalid for spatial scales smaller than 10°.

A. Schmittner (✉) · C. Appenzeller · T. F. Stocker
Climate and Environmental Physics,
Physics Institute, University of Bern,
Sidlerstr. 5, CH-3012 Bern, Switzerland
E-mail: schmittner@climate.unibe.ch

1 Introduction

On the global scale the atmospheric branch of the water cycle has, among others, two important impacts on the climate system. First, the atmospheric hydrological cycle serves as a sink or as a source of freshwater to the underlying ocean or land surfaces. Since the deep oceanic circulation is driven by density differences and the density of seawater is mainly dependent on its temperature and salinity, evaporation tends to increase surface water density, while precipitation has the opposite effect. Hence the atmospheric hydrological cycle provides the ocean with an upper boundary condition affecting the deep oceanic (thermohaline) circulation. Second, moisture transport is associated with transport of energy. When water evaporates from a surface (e.g. the ocean), this surface is cooled by the latent heat needed for the phase change. This heat is released to the surrounding air where condensation takes place, which can occur far away from the location where the water was evaporated. Thus the atmospheric hydrological cycle also plays an important role in the global energy transport. About one half of the atmospheric meridional energy is transported in the form of latent heat. The water cycle in the atmosphere also has other impacts, for instance on the radiation balance, but these effects are not discussed in this study. Here we concentrate on the large-scale transport of water vapor in the atmosphere and study parametrisations of this transport used in simplified climate models.

The primary tools to model the behaviour of the large-scale climate system are three-dimensional general circulation models (GCMs). However, since integrations of fully coupled atmosphere-ocean GCMs are computationally expensive, there is still a need for simpler models. One class of such models are zonally averaged climate models, which are appropriate for sensitivity studies or long time integrations. Zonally and vertically averaged energy balance models (EBMs) have already been proposed by Budyko (1969) and Sellers (1969). In

these one-dimensional models the vertically integrated temperature has been related to the near-surface temperature, which is the only prognostic variable. The radiative equilibrium at the top-of-the-atmosphere results in a net energy gain in the tropics due to the strong shortwave heating by solar radiation and a net energy loss at high latitudes due to thermal radiation. This implies a poleward energy transport in the ocean-atmosphere system. The meridional energy transport in EBMs has to be parametrised in terms of the temperature. Budyko (1969) and Sellers (1969) made the assumption that the poleward heat flux acts like a diffusive process and that it is proportional to the meridional temperature gradient. Lorenz (1979), using meteorological data, investigated the correlation between the meridional temperature gradient and the sensible heat flux. He found the assumption valid for the long-term average and the seasonal cycle of the largest spatial scales. Stone and Miller (1980) examined the relation between different components of the meridional energy fluxes and the near-surface temperature gradient using observational estimates for the Northern Hemisphere. They found good correlation between the seasonal changes of the total and sensible atmospheric heat transport and the near-surface temperature gradient. Additionally Stone and Miller (1980) examined exponents n at different latitudes assuming that the meridional transport due to transient eddies is nonlinear coupled to the near-surface temperature gradient. Such nonlinear relationships have later been developed for the use in zonally averaged dynamical-statistical models, relying on baroclinic instability theory (e.g. Branscome 1983; Neeman et al. 1989; Stone and Yao 1990; Genthon et al. 1990; Gallée et al. 1991). In these latitude-height models the eddy induced meridional transport of sensible and latent heat is a complicated function of the meridional temperature gradient, the vertical stability and other parameters and therefore a function of height. Such formulations are not appropriate for vertically averaged EBMs. Nevertheless, a nonlinear relationship between the meridional fluxes and the temperature gradient will also be considered in this study.

Atmospheric EBMs have also been coupled to ocean circulation models (Stocker et al. 1992; Fanning and Weaver 1996; Lohmann et al. 1996). This is a more realistic upper boundary condition for ocean models than mixed boundary conditions, where the surface freshwater fluxes are fixed and the SST (sea surface temperature) is relaxed to climatological values. Since the atmospheric moisture transport provides an important feedback for the thermohaline circulation (e.g. Manabe and Stouffer 1993), many of these models were supplemented with a balance equation for moisture (e.g. Chen et al. 1995; Weaver et al. 1998; Stocker and Schmittner 1997). In most studies the meridional atmospheric moisture transport was parametrised analogous to the sensible heat transport as a down-gradient diffusive process. The purpose of the present work is to validate these parametrisations with reanalysis data and results from a comprehensive general circulation model. In addition, two closures for the zonal distribution of precipitation in the model of Schmittner and Stocker (1999) are tested.

Section 2 introduces the parametrisations. The database for the validation is described in Sect. 3. Sections 4 and 5 present the climatologies of the zonally averaged hydrological cycle as computed from the different datasets and the results of the validation. A discussion of the results and the uncertainties follows in Sect. 6.

2 Description of the parametrisations

2.1 Parametrisations for the meridional heat and moisture transports

In atmospheric energy balance models (e.g. Sellers 1969; North et al. 1983) the eddy diffusion parametrisation of the meridional sensible heat flux (F) is written as

$$\boldsymbol{F} = -K_T \nabla T \ , \tag{1}$$

where T is the near-surface air temperature and K_T is a latitude dependent, constant eddy diffusivity for sensible heat. The transport we term here 'sensible' heat flux is actually the flux of internal energy plus potential energy (see Appendix). In EBMs these two components are not distinguished. For this reason and for the sake of simplicity we use the term 'sensible' throughout.

An analogous formulation can be assumed for the moisture (or latent heat) flux (Chen et al. 1995)

$$\boldsymbol{L} = -K_q \nabla q = -K_q r \frac{\partial q_s}{\partial T} \nabla T \ , \tag{2}$$

where K_q is the constant meridional eddy diffusivity for moisture, r is the constant relative humidity, and q and q_s are the specific humidity and the saturation specific humidity, respectively. Using the above formulation negative diffusivities can occur if realistic fluxes and temperatures are applied (e.g. Lohmann et al. 1996; Chen et al. 1995).

Other authors (e.g. Genthon et al. 1990; Stone and Yao 1990) proposed a nonlinear relationship between the eddy transports and the temperature gradient. Schmittner and Stocker (1999) and Wang and Mysak (1999) included advective transport in the formulations of the meridional water vapour and sensible heat transports, which should represent the effect of the mean meridional circulation. General formulae for the parametrisation of the meridional fluxes can then be written as

$$\boldsymbol{F}_{\mathrm{adv}} = \tilde{F} - K_T \left|\frac{\partial T}{\partial y}\right|^{n-1} \frac{\partial T}{\partial y} \ , \tag{3}$$

for the sensible heat flux and

$$\boldsymbol{L}_{\mathrm{adv}} = \tilde{L} - K_q r \frac{\partial q_s}{\partial T} \left|\frac{\partial T}{\partial y}\right|^{n-1} \frac{\partial T}{\partial y} \ , \tag{4}$$

for the meridional moisture flux. The power n expresses nonlinearity whenever it is not equal one and $\tilde{F}$ and $\tilde{L}$ represent the effect of the mean meridional circulation on the sensible and latent heat flux, respectively.

Here we would like to make a note on the terms $\tilde{L}$ and $\tilde{F}$. The inclusion of these terms was originally motivated by the shortcomings of the purely diffusive approach at low latitudes. Down-gradient diffusion is expected to be the large-scale time-mean effect of atmospheric eddies. The mean meridional circulation, on the other hand, does not necessarily transport tracers down-gradient. If we assume the mean meridional circulation to consist of a lower and an upper branch, which are mainly responsible for the net fluxes, we can approximate the fluxes of moisture and internal plus potential energy (sensible heat) by the mean meridional circulation as

$$\tilde{L} \approx \Psi_{\max}/H \cdot (q_u - q_l) \ , \tag{5}$$

and

$$\tilde{F} \approx \Psi_{\max}/H \cdot (\Theta_u - \Theta_l) \ , \tag{6}$$

where $\Psi_{\max}$ is the maximum of the streamfunction Ψ in m^2/s, defined as $v = -\partial\Psi/\partial z$. H denotes the height of the atmosphere, q is the specific humidity, Θ is the potential temperature and the subscripts l and u indicate mean values in the lower (planetary boundary layer) and upper (upper troposphere) branches of the zonally averaged circulation, respectively. Since the specific humidity decreases exponentially with height q_u can be neglected. If $\Psi_{\max}$ is taken proportional to the low level meridional wind velocity v we can approximately write

$$\tilde{L} = v_q q_l \ , \tag{7}$$

with the advection velocity for moisture $v_q = \alpha_q v$, that is proportional to the near surface wind velocity with the constant dimensionless factor α_q. The specific humidity can again be expressed in terms of temperature $q = rq_s(T)$, assuming a constant relative humidity r.

For the transport of internal and potential energy one cannot neglect Θ_u and thus the effect of the mean meridional circulation on the sensible heat flux must be treated differently. Here we propose two simple alternatives to deal with the sensible heat flux by the mean meridional circulation. The first assumes a constant difference in potential temperature between the upper and lower branches $\Delta\Theta = \Theta_u - \Theta_l$. Then we can express the flux by the mean flow as

$$\tilde{F}_1 = \alpha_T \Delta\Theta v \ , \tag{8}$$

where α_T is a constant dimensionless factor. Second we regard the mean circulation as providing a background meridional flux

$$\tilde{F}_2 = F_0 \tag{9}$$

that does not vary in time.

2.2 Closures for the zonal distribution of precipitation

In their coupled ocean-atmosphere model Schmittner and Stocker (1999) use two different closures for the zonal distribution of precipitation. Their atmospheric EBM component diagnoses the zonally averaged precipitation P from a steady state balance equation for specific humidity. This EBM is coupled to a three-basin, zonally averaged ocean model. At some latitude bands more than one ocean basin underlays one atmospheric cell. This geometry made it necessary to compute the precipitation $p_n(\phi)$ into basin n at latitude ϕ from the zonal mean value $P(\phi) = \sum_{n=1}^{3} (\Delta\Lambda_n/2\pi) \cdot p_n(\phi)$, where $\Delta\Lambda_n$ is the zonal width of basin n. The following two closures (P1 and P2) have been proposed:

P1. As the standard closure the ratio $p_n/P = c_n(\phi)$ is assumed to be a constant at any latitude. This means that the relative zonal distribution of precipitation into the different basins will not change in time.

P2. The second closure is based on a split of the zonally averaged precipitation $P(t) = P_0 + P^*(t)$ into a time-mean value P_0 and the time-dependent anomaly $P^*(t)$. The precipitation into basin n is also split into a constant value and an anomaly, according to $p_n(t) = p_{n0} + p_n^*(t)$. The assumption is now that the zonally averaged anomaly P^* is equally distributed into the different basins, which leads to $p_n^* = 2\pi P^*/\sum_{i=1}^{3} \Delta\Lambda_i$ for all n.

Because these closures are arguably ad-hoc, it is necessary to assess their validity based on 3-dimensional datasets.

3 Database

The database for the validation consists of four alternative datasets. First, GCM results from the ECHAM3 atmosphere model were applied to examine externally forced changes in different steady states for the long-term mean. The GCM results consist of five-year mean monthly data from a control run and from a doubling CO_2 experiment with a high horizontal resolution (T106, corresponding to a 1.1° grid spacing) atmosphere model. Both experiments included the seasonal cycle. The $2\times CO_2$ run was designed as a time-slice experiment (Wild et al. 1997), where SST and sea ice boundary conditions were taken from a lower resolution (T21, corresponding to a 5.6° grid spacing), coupled atmosphere-ocean model (ECHAM1-LSG) experiment. The global mean temperature rise at 2 m is 1.5 K, and therefore the climate sensitivity is in the lower range of that reported by the IPCC (Houghton et al. 1996).

The interannual and seasonal variability was explored using reanalysis data. This was necessary since global observations of surface fluxes are not available for a sufficiently long time span. The 15-year reanalysis dataset from the European Center for Medium Range Weather Forecast (ECMWF), referred to as ERA15 in the following and 39-years of National Center for Environmental Prediction (NCEP) reanalysis data were applied. The ERA15 data (Gibson et al. 1997) have a high horizontal resolution of $\sim 1.1° \times 1.1°$ and cover the years from 1979 to 1993. From NCEP (Kalnay et al. 1996) monthly mean data from the 39-year period from 1958 to 1996 on a $2.5° \times 2.5°$ grid were taken. We used vertical heat fluxes at the surface and at the-top-of-the-atmosphere, air temperature at 2 m, precipitation and evaporation rates. From NCEP, additionally, pressure level data of temperature, specific humidity and geopotential height were used to calculate the energy storage during the annual cycle. All fluxes were calculated using forecast data. Unlike the sea level pressure or the sea surface temperature the vertical heat fluxes, precipitation and evaporation are model-derived fields and thus depend on various physical parametrisations (Kalnay et al. 1996).

From the reanalyses the meridional sensible and latent heat fluxes were computed by integrating the vertical fluxes at the surface and at the top of the atmosphere as described in the appendix. Since the vertical fluxes are part of the forecast models they are not directly constrained by observations. Inconsistencies of the forecast part of the reanalysis datasets, which will be mentioned in the next section, made it desirable to apply another dataset. This dataset consists of annual mean meridional sensible and latent heat fluxes for the 20-year period from 1978 to 1997. The fully 4-dimensional, twice daily assimilated data from the NCEP reanalysis were used for this purpose. Meridional sensible and latent heat fluxes at all pressure levels below 100 hP were vertically and zonally integrated and annually averaged. The method is described in detail in Masuda (1988). This dataset will be referred to as 4DDA (four-dimensional data assimilation).

4 Results for the transport parametrisations

The computation of the meridional heat transports from the surface and top-of-the-atmosphere vertical fluxes is described in detail in the appendix. In order to obtain zero meridional fluxes at the North Pole, one has to adjust the fluxes to force a global mean zero. This has been done by subtracting the global mean from the integrands in Eqs. (A1) and (A2). These global imbalances should be much smaller than the net fluxes themselves, since the global integration, even of a relatively small imbalance, results in considerable corrections of the fluxes. Other methods of adjusting the fluxes, i.e. multiplying the outgoing longwave radiation at the top-of-the-atmosphere or the precipitation with a constant factor have also been checked, but showed similar fluxes and did not alter the results reported.

An overview of the imbalances and the individual terms contributing to them is given in Table 2 together with estimates from Kiehl and Trenberth (1997). Generally, the global mean values are in reasonable agreement for the different datasets. Differences of about 10 W/m^2 occur. At the top-of-the-atmosphere and for the hydrological cycle the ECHAM3 fluxes are better balanced, while the surface fluxes are more in balance for the reanalyses data. The magnitude of the imbalances gives an indication of the reliability of the computed fluxes. Small imbalances add confidence to the computed fluxes, while for large imbalances the method of adjusting the fluxes introduces large uncertainties and hence it will be inappropriate. The imbalances and their variation in time will also be the criterion in choosing the appropriate dataset for the validation of the seasonal and interannual variability.

Figure 1 shows the atmospheric meridional heat fluxes averaged over the time period of each individual dataset. Although their shapes are similar, the absolute values of the fluxes show considerable differences. For instance, the sensible heat flux in the Southern Hemisphere is up to twice as large in the ERA15 reanalysis than that from the 4DDA data. ECHAM3 and NCEP sensible heat fluxes are quite similar and fall between the larger ERA15 and the smaller 4DDA values.

Since we are only interested in large spatial scales, the fluxes as well as the near-surface temperatures were mapped on a 10° latitudinal grid. We then calculated the diffusivities for the sensible and latent heat fluxes by solving Eqs. (1) and (2) for the diffusivities. The sensible and latent heat fluxes in watts as shown in Fig. 1 had to be divided by $2\pi a C_p \rho_A H_T \cos(\phi) = \cos(\phi) 4.096 \cdot 10^{14}$ J/(mK) and $2\pi a L_0 \rho_A H_q \cos(\phi) = \cos(\phi) 2.207 \cdot 10^{17}$ J/m, respectively in order to obtain the fluxes from Eq. (1) in Km/s and Eq. (2) in m/s. See Table 1 for a description of the various constants and for the applied values.

4.1 Mean state

Figure 2 shows the diffusivities for the latent and sensible heat transport calculated from the 15-year mean ERA15 data and from the 5-year mean data from the ECHAM3 control run. Diffusivities calculated from the other datasets are similar to the ones shown in Fig. 2. Both datasets show positive values for the diffusivity of sensible heat at all latitudes. The order of magnitude of the diagnosed diffusivities ($10^6\,m^2/s$) is consistent with other estimates (e.g. Stocker et al. 1992; Chen et al. 1995; Fanning and Weaver 1996). Both datasets show an order of magnitude higher diffusivities near the equator with the absolute maximum at 5°N. This is an indication that in the tropics the eddy diffusivity parametrisations break down. This is particularly evident for the latent heat flux, which is directed up the temperature gradient

Table 1 Notation

$a = 6.371 \cdot 10^6$ m	Radius of the Earth
$C_p = 1004$ J kg^{-1} K^{-1}	Heat capacity of air
$\rho_A = 1.225$ kg m^{-3}	Air density
$\rho_* = 1002$ kg m^{-3}	Reference water density
$H_T = 8,320$ m	Atmospheric scale hight for temperature
$H_q = 1,800$ m	Atmospheric scale hight for humidity
$L_0 = 2.5 \cdot 10^6$ J kg^{-1}	Latent heat of evaporation

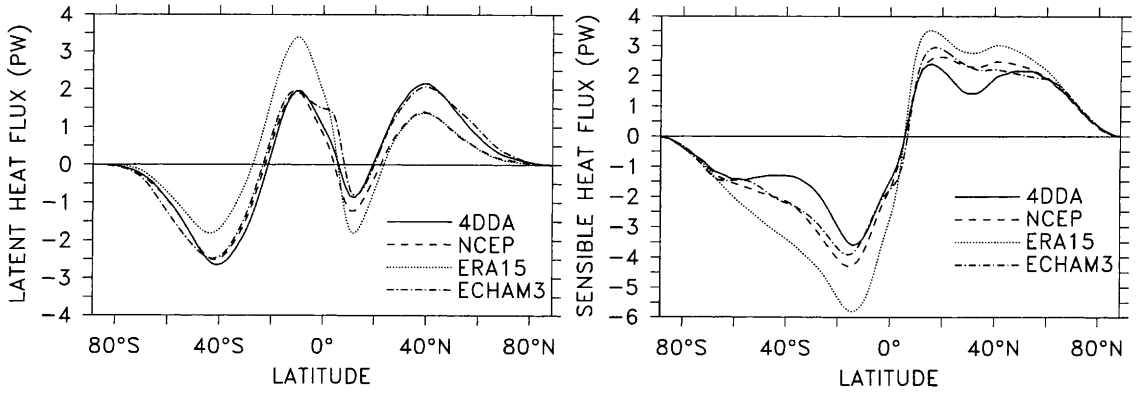

Fig. 1 Atmospheric meridional latent (*left*) and sensible (*right*) heat fluxes in PW ($1PW = 10^{15}W$) as calculated from the 4DDA (*solid*), NCEP (*dashed*), ERA15 (dotted) and ECHAM3 (*dash-dotted*) datasets

Table 2 Globally averaged heat fluxes and imbalances (W/m^2). Noted are the net solar radiation (*TSR*), net thermal radiation (*TTR*) and their difference (HF^{toa}) at the top-of-atmosphere, the net solar radiation (*SSR*), net thermal radiation (*STR*), sensible heat flux (*SSH*), latent heat flux (*SLH*) and their differences (HF^{AO}) at the surface, the imbalance of the hydrological cycle ($E - P$) and the estimates from Kiehl and Trenberth (1997) (KT)

Dataset	*TSR*	*TTR*	HF^{toa}	*SSR*	*STR*	*SSH*	*SLH*	HF^{AO}	$E - P$
ERA15	238	248	10	152	55	14	85	2	3
NCEP	226	236	10	161	62	16	82	3	2
ECHAM3	235	238	3	164	63	14	84	4	0
KT	235	235	0	168	66	24	78	0	–

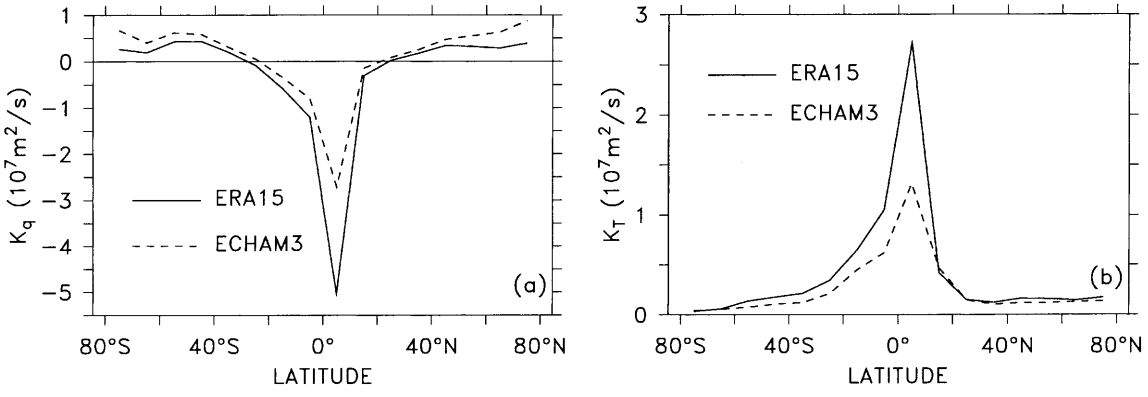

Fig. 2 Eddy diffusivities for the meridional moisture transport K_q (a) and for the meridional transport of sensible heat K_T (b) as a function of latitude as diagnosed from the ERA15 (*solid*) and ECHAM3 (*dashed*) datasets

in the tropics, and thus the diagnosed diffusivities are negative. At mid and high latitudes, however, the diffusive approximation yields positive values of the diffusivity for the moisture transport. Where negative values of the diffusivities for the moisture transport occurred, we set them to the small positive value of 10^5 m^2/s and diagnosed an advection velocity by solving Eq. (4) with $n = 1$ and Eq. (7) for v_q. The velocities diagnosed from the two datasets are shown in Fig. 3. Due to the fact that the moisture transport is mostly restricted to the lower levels, the diagnosed velocity v_q could be interpreted as low level winds. Indeed the direction and order of magnitude is consistent with annual mean near-surface wind velocities, which are also shown in Fig. 3. For the constant α_q we find positive values around 0.5 in the tropics.

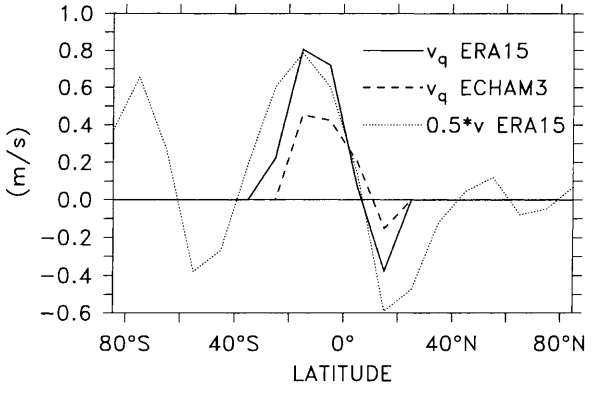

Fig. 3 Advection velocities for the parametrisations Eq. (4) as diagnosed from the ERA15 and ECHAM3 data. Annual mean 10 m meridional wind velocity (multiplied by 0.5) from the ERA15 dataset is given for comparison (*thin dotted*)

4.2 Long-term variability

The ability of the parametrisations to simulate an atmospheric mean state that is different from the present one was assessed using results from the ECHAM3 CO_2-doubling experiment. Figure 4 shows the changes of the meridional sensible and latent heat fluxes from this experiment together with the fluxes computed with Eqs. (1)–(4) using the diffusivities and the advection velocity v_q from the control run and $n = 1$. The meridional latent heat flux increased at all latitudes by about ~10% (up to 0.2 PW). Both parametrisations capture well the general shape and magnitude of the changes in water vapour flux. The inclusion of an advective transport in the parametrisation improves the agreement with the GCM results in the tropics considerably. Mainly responsible for the changed water vapour flux in the parametrisation is the strong temperature dependence of the Clausius-Clapeyron term $\partial q_s/\partial T$ in Eq. (2) (Schmittner and Stocker 1999).

The poleward sensible heat flux has decreased at mid and high latitudes in the global warming experiment up to 0.15 PW (~10%). This feature is crudely captured by

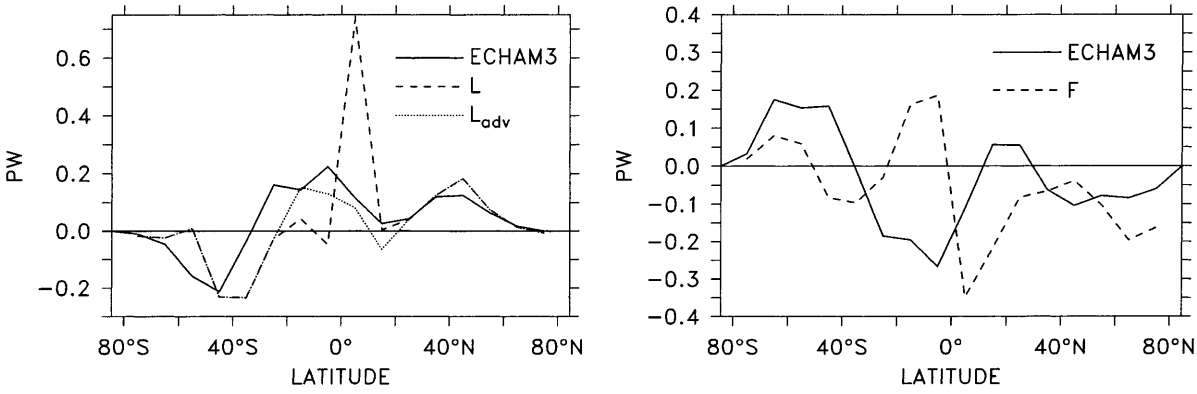

Fig. 4 Meridional profiles of the changes in northward latent (*left*) and sensible (*right*) heat fluxes between the ECHAM3 control run and the $2 \times CO_2$ experiment (*solid*). Results from the parametrisations (Eqs. 1–4) without (*dashed*) and with (*dotted*) advective transport were computed using the diffusivities from the control run, shown in Fig. 2 as dashed lines. Annual mean data have been used in the calculations

the purely diffusive parametrisation, while the changes between 10°N and 30°S are not well represented. The largest errors occur at 5°S and 10°S, where the parametrisation shows decreased southward transport due to a lower temperature gradient there. This clearly shows the limits of the parametrisations, which cannot account for possible changes in the Hadley circulation or in the lapse rate and the implied changes of the sensible heat transport at low latitudes. The inclusion of a term representing the mean circulation (Eq. 8) in the parametrisation of the sensible heat flux would show no changes in the meridional transport between the control and $2\times CO_2$ climate, since the parameter $\alpha_T \Delta\Theta$ and the velocity v, would have to be taken from the control run.

Nonlinear parametrisations have also been tested. Therefore, we used Eqs. (3)–(4) with $n = 2$. Since we found qualitatively similar results as for the linear parametrisation, plots are not presented. Additionally, both linear as well as nonlinear ($n = 2$) parametrisations have been applied to the full seasonal cycle. Again we only show results from the linear parametrisation because of the minor differences between the parametrisation results for $n = 1$ and $n = 2$. The parameters K_q, K_T, α_q, $\alpha_T \Delta\Theta$ and F_0, shown in Fig. 5, have been objectively determined from the control run, with seasonally varying meridional near surface wind velocity v. This has been done by minimizing the squared differences of the parametrisations and the GCM fluxes. The present-day seasonal cycle can be reasonably well reproduced by the parametrisations. Then the fluxes have been computed for the warmer climate using these parameters and monthly temperature data from the ECHAM3 $2\times CO_2$ run. Note that for parametrisations $\tilde{L}$ and $\tilde{F}_1$ the velocity v has been taken from the control run, since in a non dynamical model the changes in velocity cannot be predicted. In Fig. 6 the annual mean results of the seasonal performance of the parametrisations are shown together with the GCM results. Similarly good results as for the annual mean performance of the parametrisation (Fig. 4) are obtained for the latent heat flux. The peak at 15°S is due to the high diffusivity diagnosed at that latitude (see Fig. 5). Similar peaks for the sensible heat flux are obtained for the parametrisation with $\tilde{F}_2$ at 5°S and 5°N. These are also due to the high diffusivities diagnosed at these latitudes. Generally, the parametrisations of the sensible heat flux yield similar results for the seasonal performance as for the annual mean. The better agreement of parametrisation $\tilde{F}_1$ with the GCM output at 15°S, 5°N and 25°N is due to the negative diffusivities diagnosed there (see Fig. 5). At these latitudes the GCM predicts an increased poleward sensible heat flux and a decreased meridional temperature gradient. Negative diffusivities are not only a problem in numerical models, where they can lead to instabilities, but also difficult to interpret physically in the sense of eddy induced diffusion. Thus the good agreement of parametrisation $\tilde{F}_1$ with the GCM results should not obscure the fact that the changed sensible heat flux at low latitudes can hardly be explained by any of the parametrisations used in this study.

4.3 Interannual variability

The year-to-year variations of the meridional sensible and latent heat fluxes computed from the two reanalyses show considerable differences. To illustrate this, we plotted the anomalies of the annual mean latent heat flux from 1979 to 1993 as computed from the ERA15 surface fluxes, from the NCEP surface fluxes and the corresponding anomalies from the 4DDA data in Fig. 7. The ERA15 data show the largest variability with maxima of 1.5 PW. The anomalies of the latent heat flux computed from the vertical NCEP fluxes and the 4DDA anomalies compare well with each other and show amplitudes much smaller than those from the ERA15 data. Part of the large variability found in the ERA15 fluxes is introduced somehow artificially due to the correction applied to the unbalanced vertical fluxes year by year. Interannual variations of the globally averaged vertical freshwater flux $E - P$ are much larger for the ERA15 than for the NCEP reanalysis. For ERA15 they amount

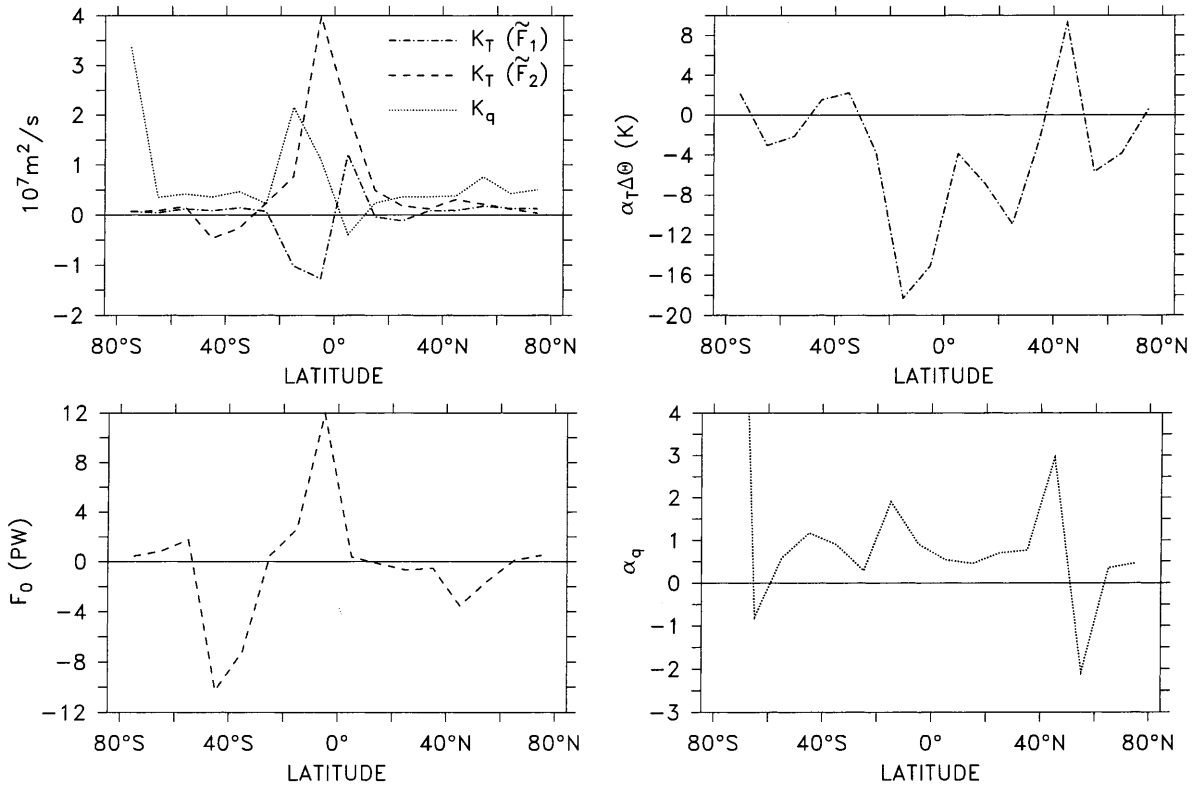

Fig. 5 *Top left*: Eddy diffusivities for latent heat K_q and for sensible heat K_T as a function of latitude. The diffusivities for sensible heat have been calculated for two parametrisations of the mean meridional transport $\tilde{F}_1$ (Eq. 8) and $\tilde{F}_2$ (Eq. 9). *Top right*: $\alpha_T \Delta\Theta$ for the parametrisation $\tilde{F}_1$. *Bottom left*: F_0 for the parametrisation $\tilde{F}_2$. *Bottom right*: α_q for the parametrisation $\tilde{L}$ (Eq. 7). All parameters were calculated objectively by minimizing the squared difference between the parametrisations and the seasonal cycle of the ECHAM3 control run

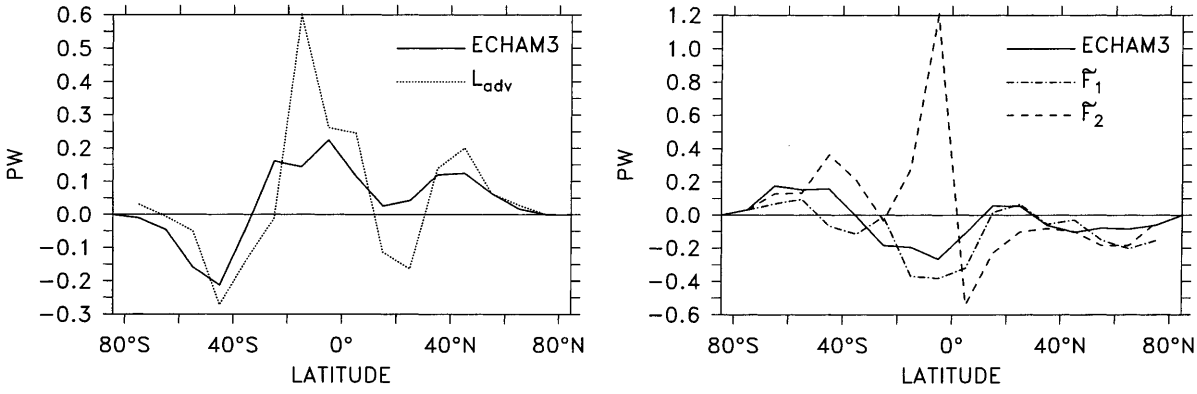

Fig. 6 Same as Fig. 4 but the full seasonal cycle has been used for the calculations. The parameters K_q, K_T, α_q, $\alpha_T \Delta\Theta$ and F_0 have been calculated from the control run and are shown in Fig. 5. Note that for the parametrisations including a seasonally varying near surface meridional wind velocity v (Eqs. 7 and 8) this has been taken from the control run

to a peak-to-peak variation of about 13 W/m^2, while for the NCEP overall variation is only about 2 W/m^2. Highest values of about 2–4 W/m^2 for globally averaged $E - P$ in ERA15 occur in the years 1982 to 1984, when the meridional latent heat flux shows positive anomalies in the Northern Hemisphere and negative anomalies in the Southern Hemisphere. Lowest values of global mean $E - P$ (-5 to -9 W/m^2) in the years 1989 to 1993 correspond to the reversed latent heat flux anomaly pattern. Thus the interannual variability shown in Fig. 7 for the ERA15 fluxes is contaminated by the large variability of the $E - P$ imbalance. The good agreement of the anomalies computed from the vertical NCEP fluxes and those from the 4DDA data are probably not surprising because the 4DDA fluxes were also computed from the NCEP reanalysis, but due to the two different computation methods this result adds credibility to our method of adjusting the fluxes if the variation of the imbalances

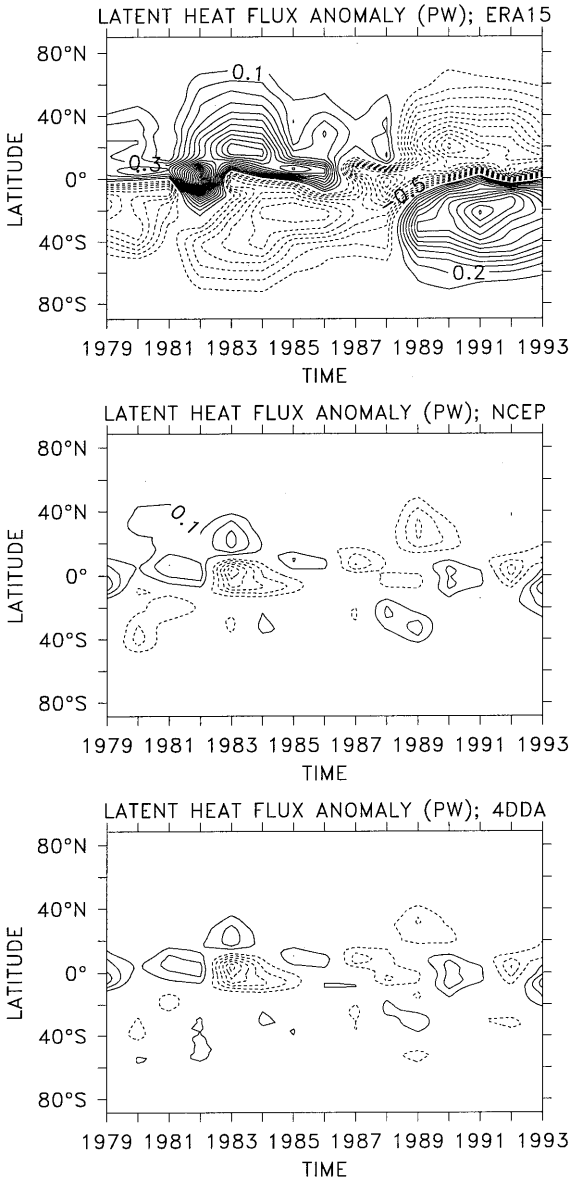

Fig. 7 Interannual variability of the latent heat flux in PW. Plotted is the difference of the annual mean flux and the 15-year average as a function of time and latitude. Results from the ERA15 (*top*), NCEP (*middle*) and from the 4DDA data (*bottom*) are plotted, contour interval is 0.1 PW and negative isolines are dashed

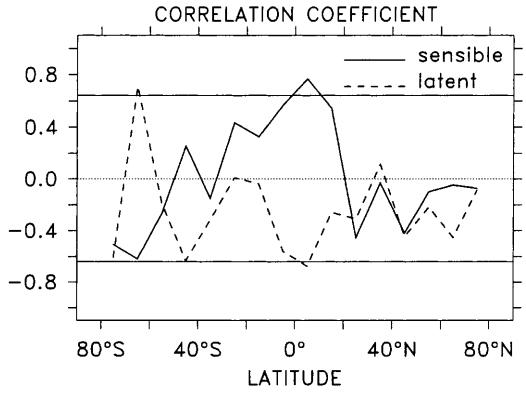

Fig. 8 Temporal correlation coefficients for the interannual variability of the meridional sensible and latent heat fluxes from the 4DDA data and those computed with the purely diffusive parametrisations (Eqs. 1 and 2) for the years 1979 to 1993. The thin horizontal lines indicate the 99% confidence level from a two sided t-student test with N-2 = 13 degrees of freedom (*solid*) and the zero line (*dotted*)

is small. On the other hand, if the imbalances vary considerably in time, like for ERA15, the method is not appropriate.

A common feature of all three datasets is the negative correlation of the sensible (not shown) and latent heat flux anomalies in the tropics. Thus enhanced northward sensible heat flux is accompanied with enhanced southward latent heat transport and vice versa. Small shifts of the intertropical convergence zone (ITCZ), where the gradients are strongest, result in large anomalies and these anomalies are of opposite sign for the sensible and latent heat fluxes.

In Fig. 8 the temporal correlation coefficients for the years 1979 to 1993 of the 4DDA data and the purely diffusive parametrisations are plotted. The parametrisations have been computed with the ERA15 temperatures, but NCEP temperatures agree well with the ERA15 temperatures and would result in nearly the same correlation coefficients. At most latitudes the correlation is below the 99% confidence level for both latent and sensible heat flux. Thus, it is obvious that the parametrisations are not appropriate for interannual variations of the heat fluxes. The parametrisations show an order of magnitude too large variability in the tropics and more than an order of magnitude too small variability in mid and high latitudes when compared with the 4DDA data. Other parametrisations, including the influence of the mean meridional circulation (Eqs. (7–9)) have also been tested. Since the velocities v must be taken to be seasonally fixed and F_0 is also time-independent, interannual variations in the mean meridional circulation cannot be reproduced. Thus, the results are similar to those of the purely diffusive parametrisation. Here we choose the 4DDA data for the validation because they are not affected by the imbalances. However, the result is independent of the applied dataset. Correlation coefficients computed with the ERA15 and NCEP fluxes are similar.

4.4 Seasonal variability

The calculation of the meridional heat fluxes in the previous sections are all based on the assumption of stationarity, i.e. storage terms are neglected in the balance equations. This approach might be no longer appropriate if the seasonal variability is considered. In order to account for the heat and moisture storage during the seasonal cycle, the calculation of the meridional transports must include the storage terms (i.e. the last terms in the parenthesis of Eqs. A1 and A2). In order to examine the relative importance of the storage terms we plotted the mean seasonal cycle of

the fluxes computed with the correction due to the storage term minus the fluxes computed without the correction from the NCEP dataset in Fig. 9. Generally the influence of the storage term is relatively small but clearly not negligible. For the latent heat flux the maximum deviation is 0.7 PW, which is about 15% of the maximum seasonal variation of the meridional latent heat flux. For the sensible heat flux the influence of the storage term is even stronger with values of up to 2 PW corresponding to 30% of the maximum seasonal variation.

The mean seasonal cycle of the northward sensible and latent heat fluxes computed from the NCEP data including the storage terms are shown in Fig. 10 as monthly anomalies from the annual mean. We decided here to use the NCEP data because they show smaller month-to-month variations of the global imbalances than the ERA15 dataset. For NCEP the difference between the minimum and the maximum imbalance in $E - P$ accounts for about 2.5 W/m^2, while it is about 11 W/m^2 for ERA15. However, the anomalies computed with NCEP compare well with those from ERA15 with the following differences: (1) both sensible and latent heat flux anomalies from ERA15 show 20% higher amplitudes in the tropics; (2) the local minimum at 35°S in the NCEP sensible heat flux anomalies is not present in the ERA15 data; (3) the phase of the variations of the latent heat flux in mid and high latitudes is somewhat different while the variance is similar. The NCEP fluxes compare also favourably with the fluxes computed from the ECHAM3 control run. As shown in Fig. 10 the poleward flux of sensible heat is stronger in winter and weaker in summer at all latitudes. Maxima of the variations occur at low latitudes with differences between summer and winter of more than 10 PW. The amplitude of the variation is smaller at mid and high latitudes and it is stronger in the Northern than in the Southern Hemisphere extra tropics. This is most probably related to the stronger annual temperature variations in the Northern Hemisphere due to the unequal distribution of land masses. The latent heat flux is anticorrelated with the sensible heat flux at low latitudes with about 30% smaller amplitude. At mid and high latitudes the variations of the latent heat flux are much

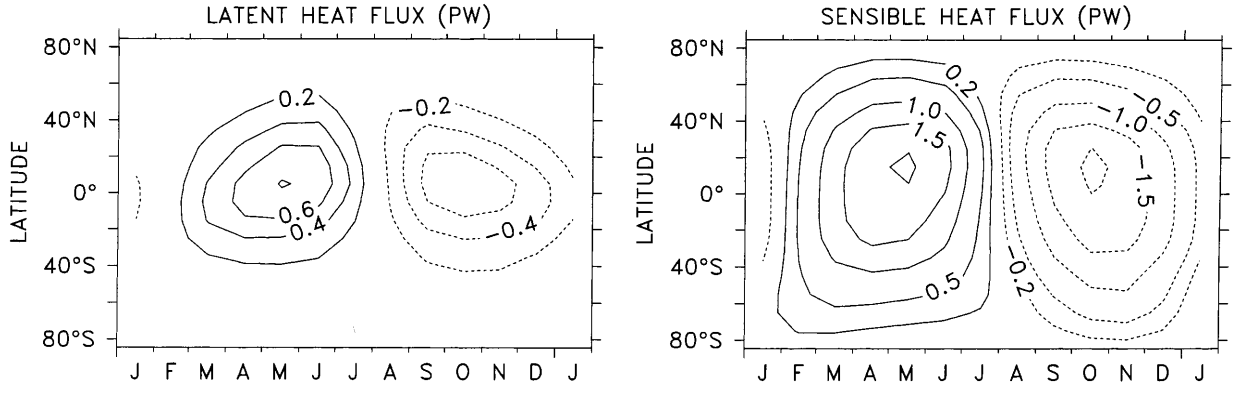

Fig. 9 Influence of the storage terms in the calculation of the seasonal variability of the meridional latent and sensible heat fluxes. The difference of the corrected and uncorrected fluxes calculated from the mean seasonal cycle of the NCEP reanalysis is given as a function of time and latitude in PW. Dashed isolines correspond to negative values and contour interval is 0.2 PW for the latent heat flux (*left*) and 0.5 PW for the sensible heat flux (*right*) with additional isolines at ± 0.2 PW

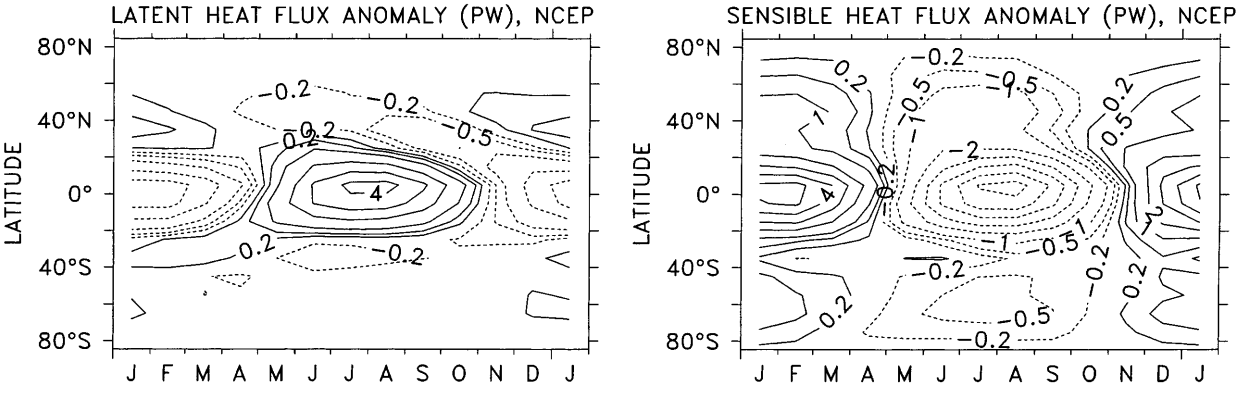

Fig. 10 Seasonal variability of the latent (*left*) and sensible (*right*) heat fluxes in PW. The mean seasonal anomaly is given as a function of month of year and latitude based on the NCEP reanalysis (contour interval is 1 PW with additional isolines at ± 0.5 PW and ± 0.2 PW). The fluxes from the NCEP dataset were computed including the influence of heat and moisture storage (see Eqs. A1 and A2)

smaller than those of the sensible heat flux. This is due to two opposing effects. The increased circulation in the winter hemisphere tends to increase the moisture transport, while the lower temperatures lead to a smaller capability of the air to hold and transport water vapour.

Now we calculate the present-day seasonal cycle simulated by the parametrisations. Since the mean meridional circulation and the surface meridional wind velocities show strong variations during the seasonal cycle, the application of constant meridional velocities v would lead to unrealistically small variability particularly at low latitudes. Instead, we use the observed meridional near surface wind velocity taken from the reanalysis, and diagnose the parameters α_T, $\alpha_q\Delta\Theta$ and F_0 as well as the diffusivities K_q and K_T from the mean seasonal data. These parameters have been calculated by minimizing the squared differences between the parametrisations and the reanalysis data and are similar to the ones diagnosed from the ECHAM3 control run as shown in Fig. 5. The seasonal cycle simulated with these parameters is shown in Fig. 11 as anomalies from the annual mean. Comparison of the fluxes with Fig. 10 shows good agreement between the parametrisations and the reanalysis data.

Similar results are obtained by applying a nonlinear parametrisation with $n = 2$ including the same terms for the mean transport. One has to keep in mind that for the calculation of the parameters ($\alpha_T\Delta\Theta$, α_q, F_0, K_T, K_q) information from the seasonal variations has been used. If only annual mean information is used, the performance of the parametrisations would be worse.

The reliability of the results presented in this section depends on the accuracy of the calculated sensible and latent heat fluxes (Fig. 10). We suggest that the confidence in the seasonal variation is higher where the variations are large and lower where small annual variations occur. Thus, the confidence in the calculated sensible heat flux is high at all latitudes except at 35°S, while for the latent heat flux the confidence is high only at low latitudes. Generally the fluxes are more reliable in the Northern Hemisphere than in the Southern Hemisphere, because the quality and spatial coverage of the observational input to the reanalysis model is better there.

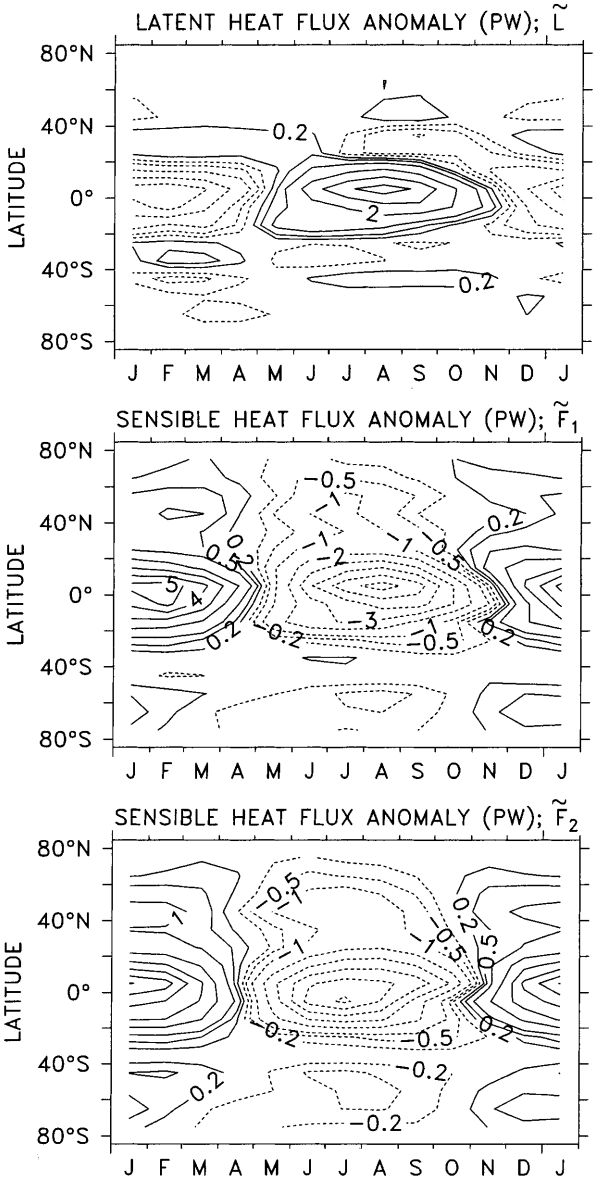

Fig. 11 Seasonal variability of the latent and sensible heat fluxes in PW as calculated from the parametrisations (Eqs. 3 and 4) with n = 1. *Top*: Latent heat flux (Eq. 4 with 7). *Middle*: Sensible heat flux using Eq. (3) with $\tilde{F}_1$ (Eq. 8). *Bottm*: Sensible heat flux using Eq. (3) with $\tilde{F}_2$ (Eq. 9). The applied diffusivities, and α_q and $\alpha_T\Delta\Theta$ and F_0 are similar as those shown in Fig. 5. The mean seasonal anomaly is given as a function of month of year and latitude (contour interval is 1 PW with additional isolines at ± 0.5 PW and ± 0.2 PW)

4.5 Spatial scale limitations

In order to examine the validity of the parametrisations with respect to the spatial scales we apply different latitudinal grid spacings. The variables are averaged on a 20°-grid, on a 5°-grid and additionally the parametrisations were tested on the original data grids, which correspond to a spacing of approximately 1.1°. To test the influence of the spatial scales on the long-term variability we computed the changes of the sensible and latent heat fluxes between control and $2\times CO_2$ climate as shown in Fig. 4 but on the different latitudinal grids. In Table 3 the latitudinal correlation coefficients for the changed fluxes from ECHAM3 and those changes calculated with the parametrisations are listed. For the 10°-grid, for instance, this is the correlation between the curves in Fig. 4. Generally the correlation decreases for smaller spatial scales for the purely diffusive parametrisations ($\boldsymbol{F}$ and $\boldsymbol{L}$), while it changes less for the formulations including the mean circulation ($\boldsymbol{F}_{\mathrm{adv}}$ and $\boldsymbol{L}_{\mathrm{adv}}$). This is due to very large values (of both signs) of the diffusivities diagnosed in the tropics and at high latitudes for the small-scale grids. At these latitudes the fluxes

calculated with the parametrisations also show very large variations. The limitation of the diffusivities also reduces the amplitude of those variations and therefore improves the correlation. However, for the 1° grid spacing all parametrisations show much more smaller-scale latitudinal variability compared to the relatively smooth GCM results (not shown). Therefore, we conclude that the parametrisations should not be used for latitudinal scales smaller than 10°. An evaluation of the parametrisations on different spatial scales for the seasonal cycle also showed that the diffusive assumptions become invalid for small scales.

Table 3 Latitudinal correlation coefficients for the differences of the meridional sensible and latent heat fluxes between the control run and the doubling CO_2 experiment from ECHAM3 and those computed with the parametrisation Eqs. (1)–(4) for different spatial resolutions. $\boldsymbol{F}$ and $\boldsymbol{L}$ denote the purely diffusive parametrisations of the sensible (Eq. 1) and latent (Eq. 2) heat fluxes, respectively, while $\boldsymbol{F}_{adv}$ and $\boldsymbol{L}_{adv}$ are the parametrisations including advective transport (Eqs. (3) and (4))

$\Delta\phi$	20°	10°	5°	1°
$\boldsymbol{F}$	0.54	0.38	0.22	0.14
$\boldsymbol{F}_{adv}$	0.53	0.56	0.49	0.42
$\boldsymbol{L}$	0.90	0.54	0.44	0.17
$\boldsymbol{L}_{adv}$	0.90	0.71	0.71	0.67

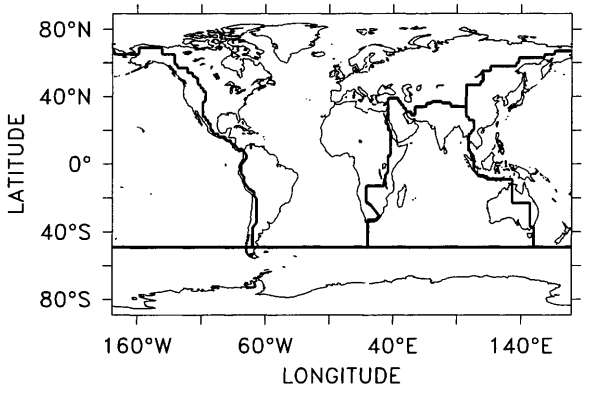

Fig. 12 Drainage basins for the Atlantic, Pacific, Indic and Southern oceans

5 Results for the zonal distribution of precipitation

In order to calculate the precipitation into the different ocean basins, we used two methods. The first is to consider only the precipitation over the ocean and to ignore the precipitation over land. The second is to define drainage basins and to assume that the precipitation, that falls over land, will drain into the associated basin in the same latitudinal band. All analyses reported in this section have been calculated with both methods. Since the results are insensitive to the applied method, in the following we present those results including the drainage basins. The drainage basins used in this study are shown in Fig. 12. The precipitation data were then averaged on a 10° latitudinal grid.

For the long-term changes again the GCM data from ECHAM3 were used, while for the interannual and seasonal variability ERA15 precipitation data were chosen, where the mean of the 12- and 24-h forecast values have been taken. Here we choose the ERA15 reanalysis because it has been shown that in the extratropics it is superior to the NCEP reanalysis (Stendel and Arpe 1997).

Figure 13 shows the relative zonal distribution of precipitation $c_n = p_n/P$ (see Subsect. 2.2) into the different basins for the 15-year mean ERA15 data and for the ECHAM3 control run. Both datasets show striking similarity in the zonal distribution of precipitation. At most latitudes there is more than average precipitation in the Pacific and less than average precipitation in the Atlantic Ocean.

5.1 Long-term variability

Here again we assess the ability of the closures to simulate a steady-state climate different from the one today.

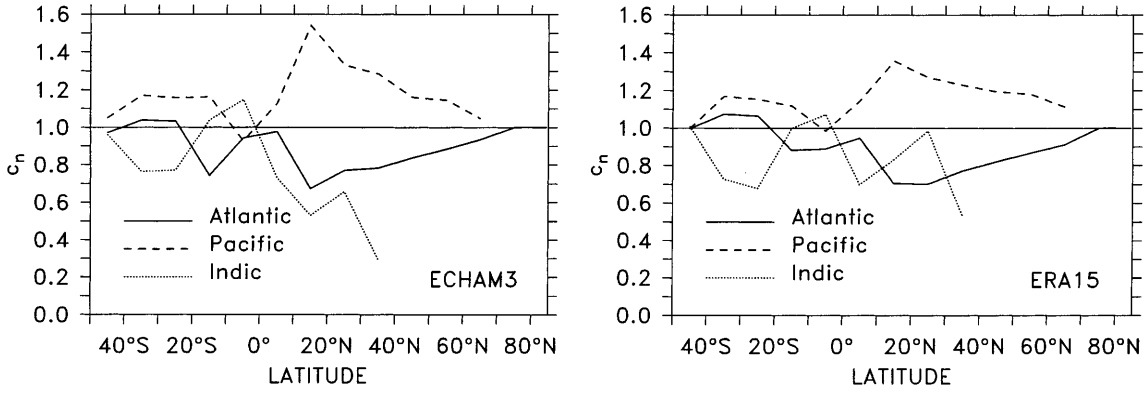

Fig. 13 Ratio of precipitation p_n into basin n (Atlantic, Pacific, Indic) to zonally averaged precipitation P as a function of latitude for the control run of ECHAM3 (*left*), and the ERA15 dataset (*right*)

In Fig. 14 the precipitation differences between the control run and the $2\times CO_2$ experiment from the ECHAM3 model are plotted together with the results of the closures P1 and P2. The results of closure P1 are calculated with the coefficients c_n from the control run as shown in Fig. 13, and for closure P2 the time-mean values P_0 and p_{n0} are taken from the control run, and the anomalies P^* and p_n^* are the differences between $2\times CO_2$ experiment and control. In general, both closures capture well the shape and magnitude of the changed precipitation patterns in the different ocean basins. The largest errors occur in the subtropical Indian Ocean, where the high precipitation anomalies cannot be captured by the closures. Another striking feature is that both closures exhibit very similar zonal precipitation distributions. This is due to the diagnosed values of c_n, which do not differ much from one (Fig. 13). If they were exactly one, the closures would be identical since the anomalies of closure P1 would then be equally distributed into the different basins. The differences of the precipitation anomalies into the different basins can therefore not be well represented by closure P1. Note that the agreement between the closures and the GCM results is particularly good in the North Atlantic. This is important as this is the 'centre of action' for large oceanic reorganizations such as simulated in global warming experiments (Stocker and Schmittner 1997).

5.2 Interannual variability

The temporal correlation coefficients between the interannual variability of the precipitation into the Atlantic, Pacific and Indian oceans as calculated from the ERA15 data and the closures is shown in Fig. 15. Note that the temporal correlation coefficients are the same for both closures (P1 and P2) since they differ only by a constant factor. The closures show good agreement with the data only in the Pacific and in the North Atlantic. The good agreement in the Pacific is due to the larger zonal width of the Pacific basin. This leads to a stronger contribution of the Pacific to the zonal mean precipitation. Since the precipitation anomalies into the different basins calculated with the closures P1 or P2 are proportional to the zonal mean, the correlation between data and closures is larger if the basin width is larger. In addition to the influence of the width of the basin we see that the correlation at some latitudes in the Atlantic is very low. The reason for the low correlation near the equator seems to be related to the El Niño-Southern Oscillation. During El Niño years precipitation anomalies are positive in the tropical Pacific, while they are negative or zero at low latitudes in the Atlantic drainage basin. For these reasons we suggest that the closures are not appropriate for interannual variability.

5.3 Seasonal variability

The seasonal variation of the precipitation into the different basins is much better captured than the interannual variability. This is evidenced by the temporal correlation coefficients between the mean seasonal cycle of ERA15 and the closures (Fig. 16) calculated on a 10°-grid (solid lines). The low correlation coefficient at 35°N in the Indian Ocean is somehow an artifact due to the applied drainage basins. In this latitudinal band only a few land areas in the Asia Minor and in the Himalaya region contribute to the averaged precipitation. The amplitudes of the anomalies computed with the closures (not shown) are also in reasonable agreement with the data. For the mean seasonal cycle we conclude that the closures are good approximations.

5.4 Spatial scales

Just as for the parametrisations of the meridional transports we analyzed the closure for the zonal distribution of precipitation on different spatial scales. While the errors of the closures become only slightly worse if smaller grid spacings are used in the long-term variability, the effect is greater for the results of the seasonal cycle. The temporal correlation between the closures and the ERA-data in the mean seasonal cycle is shown in Fig. 16 for a 5°-grid and for a 1°-grid. Already for the

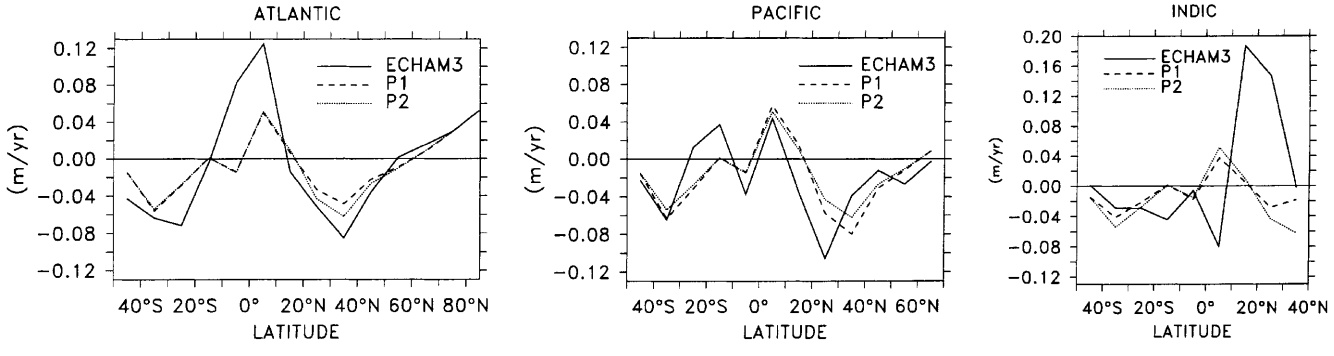

Fig. 14 Precipitation differences between the CO_2-doubling experiment and the control run of the ECHAM3 model and the results of the closures P1 and P2 as functions of latitude for the three ocean basins Atlantic (*left*), Pacific (*middle*) and Indic (*right*)

5°-grid spacing there are more latitudes at which the correlation is poor, compared with the 10°-grid spacing. The closure is obviously inappropriate for spatial scales smaller than 5°.

6 Discussion

The validation of the parametrisations in the previous sections depends on the availability and reliability of the applied data. In order to examine the ability of the parametrisations to simulate a climate different from the one today, one has to rely on GCM results, because observational estimates of meridional heat fluxes from past climates do not exist. For the long-term average we showed that the diffusive parametrisation of the moisture flux, including a mean transport in the tropics, captures well the changes simulated by a GCM under global warming conditions. The agreement is even better than that for the sensible heat flux, which is due to the occurrence of the Clausius-Clapeyron term in the parametrisation of the moisture flux. Larger errors are found for the parametrisation of the sensible heat flux, which clearly shows the limits of the simple formulations, where changes of the Hadley circulation or of the lapse rate cannot be considered.

The physical argument supporting the diffusive approximation is that on average atmospheric eddies transport properties down-gradient. This is a mixing process typical for turbulent motions. We have seen that this down-gradient transport is indeed valid at mid and high latitudes, where mainly transient and stationary eddies dominate the circulation. In the tropics, however, most of the meridional transport is due to the mean meridional circulation. Moisture is advected by the lower branch of the Hadley circulation from the subtropics, where the air is relatively dry, to the ITCZ, a region with much water vapour content. Here the water precipitates serving as a source of freshwater for the underlying ocean and land surfaces. Thus, the Hadley cell transports moisture up-gradient. This can be reasonably represented by the advective term in the parametrisation of the latent heat flux. For the sensible heat transport the parametrisation results show larger differences compared with the $2\times CO_2$ climate simulated by the GCM, particularly at low latitudes. A more realistic description of the meridional transports in the tropics must therefore include the dynamics of the Hadley circulation and take into account changes of the lapse rate. At mid and high latitudes transient eddies, arising from baroclinic instability, dominate the meridional fluxes. Here the diffusive assumption can be accepted as a 'zero-order approximation' for the long-term average and large spatial scales.

Interannual and seasonal variability was examined using reanalysis data. The meridional fluxes of moisture and sensible heat were calculated by integrating the vertical heat fluxes at the top-of-atmosphere and at the surface. NCEP and ERA15 reanalyses show some common problems in the mean vertical fluxes. For this reason we used annual-mean meridional fluxes computed from the fully 4-dimensional NCEP data. The result that interannual variability cannot be captured by

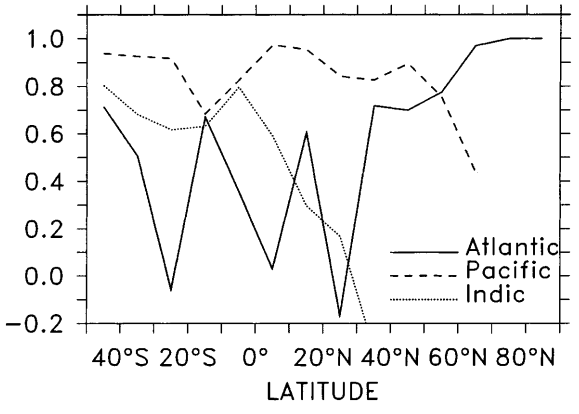

Fig. 15 Temporal correlation between ERA15 (annual mean data) derived precipitation into the different basins and that resulting from the closures

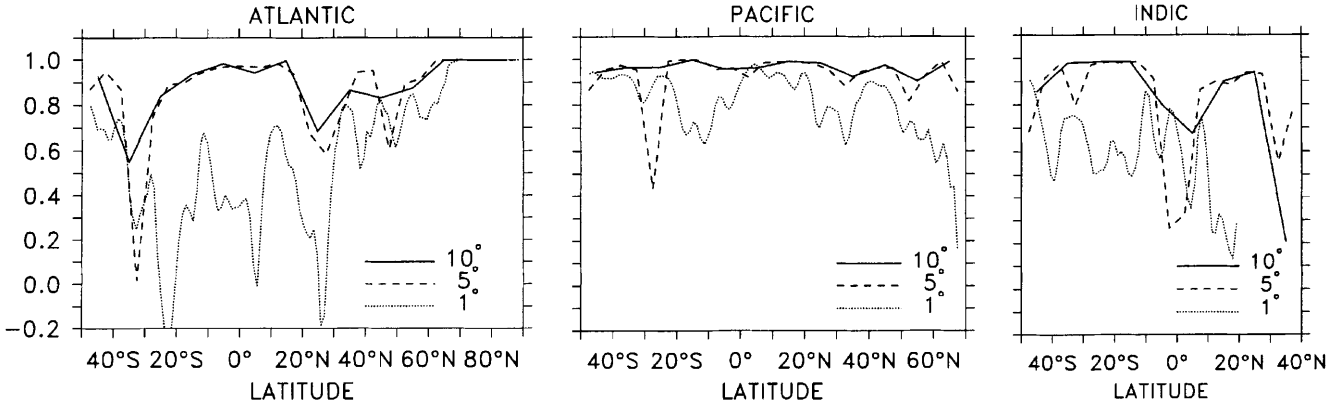

Fig. 16 Temporal correlation between ERA15 (mean seasonal cycle) derived precipitation into the different basins (*left*: Atlantic, *middle*: Pacific, *right*: Indic) and that resulting from the closures. The correlation is calculated on a 10°-grid (*solid*), a 5°-grid (*dashed*) and a 1°-grid (*dotted*)

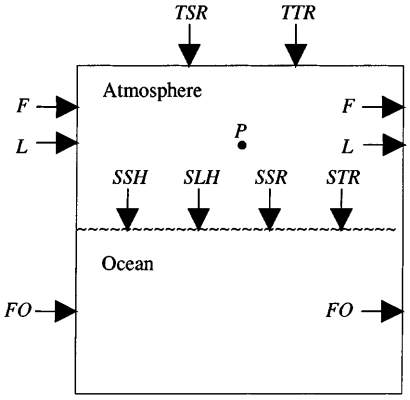

Fig. 17 Schematic of the zonally averaged vertical and meridional heat fluxes in the atmosphere-ocean system. At the top of the atmosphere the vertical fluxes are the net solar (*TSR*) and net thermal radiation (*TTR*) and at the surface the sensible (*SSH*) and latent (*SLH*) heat fluxes as well as the net solar (*SSR*) and net thermal (*STR*) radiation. The meridional transports in the atmosphere are denoted by *F* (sensible heat) and *L* (latent heat), precipitation by *P* and the meridional heat transport in the ocean is abbreviated by *FO*

the diffusive parametrisations has been common for all three datasets and is consistent with findings for the sensible heat flux (Lorenz 1979). Seasonal variations, on the other hand, can be well represented by the parametrisations. Formulations that include a seasonally varying meridional near-surface wind velocity can represent reasonably well the present-day seasonal cycle. These conclusions are independent of whether a linear or nonlinear formulation for the eddy-diffusion is used.

Interannual variability cannot be captured by any of the parametrisations presented here. Modes of the interannual variability like El Niño/Southern Oscillation or the North Atlantic Oscillation show considerable zonality. Thus, it is not surprising that zonally averaged models cannot represent this kind of climate variability.

Acknowledgements We acknowledge the constructive comments of A. Ganopolski and an anonymous reviewer, who considerably improved the paper. Equation (8) was suggested by A. Ganopolski. We are grateful to Martin Wild who provided us with the ECHAM3 data and to K. Masuda for the 4DDA data and for stimulating discussions. Thanks to the ECMWF-team for providing us with the ERA15 Reanalysis dataset. All plots have been produced with the Ferret software from NOAA. NCAR/NCEP reanalysis data have been provided through the NOAA Climate Diagnostics Center (web site at http://www.cdc.noaa.gov/). This work was supported by the Swiss national science foundation and the Swiss federal office of education and science.

Appendix: calculation of meridional heat fluxes from surface and top-of-the-atmosphere data

The meridional heat fluxes were computed indirectly by integrating the vertical fluxes at the top of the atmosphere and at the surface from the South Pole to the North Pole as described by Hastenrath (1979). The variables at the top-of-the-atmosphere (see Fig. 17) are the net solar *TSR* (top solar radiation) and the net thermal *TTR* (top thermal radiation) radiative fluxes, which are added to yield the total heat flux at the top of the atmosphere $HF^{toa} = TSR + TTR$. At the surface we consider the sensible *SSH* (surface sensible heat) and the latent *SLH* (surface latent heat) heat fluxes as well as the net solar *SSR* (surface solar radiation) and net thermal *STR* (surface thermal radiation) radiation. $HF^{bot} = SSH + SSR + STR$ is the heat flux the atmosphere 'feels' at the surface, and $HF^{AO} = HF^{bot} + SLH$ is the heat flux entering the ocean surface. All vertical heat fluxes are given in W/m^2 and are positive downward. The meridional latent (L) and sensible (F) heat fluxes can now be calculated by integration:

$$L(\phi) = a^2 \int_{\phi'=-\frac{\pi}{2}}^{\phi} \int_{\lambda=0}^{2\pi} \left(E - P - L_0 \frac{\partial \langle q \rangle}{\partial t} \right) \cos\phi' \, d\phi' \, d\lambda \ , \qquad \text{(A1)}$$

and

$$F(\phi) = a^2 \int_{\phi'=-\frac{\pi}{2}}^{\phi} \int_{\lambda=0}^{2\pi} \left(HF^{toa} - HF^{bot} + P - C_p \frac{\partial \langle T \rangle}{\partial t} - g \frac{\partial \langle z \rangle}{\partial t} \right) \cos\phi' \, d\phi' \, d\lambda \ . \qquad \text{(A2)}$$

The total precipitation and evaporation in m/s were multiplied by $L_0 \rho_* = 2.505 \cdot 10^9$ J/m^3, with the latent heat of evaporation L_0 and a reference density ρ_* as listed in Table 1 to obtain the corresponding latent heat fluxes P and E in W/m^2. Note that the surface latent heat flux multiplied by -1 is the evaporation in W/m^2. The last terms in the brackets in Eqs. (A1) and (A2) represent the storage terms of latent energy ($L_0 q$), internal energy ($C_p T$) and potential energy (gz). Vertical integrals are indicated by $\langle \psi \rangle = \int_{p_t}^{p_s} \psi \, dp/g$, where g is the acceleration due to gravity and p_s and p_t denote the surface and topmost integration limits. We use NCEP temperatures (T) and geopotential heights (z) integrated from 1000 hPa to 100 hPa for the sensible heat storage. For the moisture storage the specific humidity was averaged from 1000 hPa to 300 hPa. Here we neglected the storage of kinetic energy which is much smaller than the other terms (Oort 1971). The storage terms have only been considered in the calculation of the seasonal variability. For the interannual and long-term changes these terms have been neglected. The combined sensible and latent heat storage rate for the mean seasonal cycle computed as described above compares favorably with estimates for the Northern Hemisphere based on radiosonde data (Oort and Vonder Haar 1976).

References

Branscome LE (1983) A parametrization of transient eddy heat flux on a beta-plane. J Atmos Sci 40: 2508–2521

Budyko MI (1969) The effect of solar radiation variations on the climate of the Earth. Tellus 21: 611–619

Chen D, Gerdes R, Lohmann G (1995) A 1-d atmospheric energy balance model developed for ocean modelling. Theoret Appl Climatol 51: 25–38

Fanning AF, Weaver AJ (1996) An atmospheric energy-moisture balance model: climatology, interpentadal climate change, and coupling to an oceanic general circulation model. J Geophys Res 110: 15 111–15 128

Gallée H, Van Ypersele JP, Fichefet T, Tricot C, Berger A (1991) Simulation of the last glacial cycle by a coupled, sectorially averaged climate-ice sheet model. 1. The climate model. J Geophys Res 96: 13 139–13 161

Genthon C, Le Treut H, Jouzel J, Sadourny R (1990) Parametrization of eddy sensible heat transports in a zonally averaged dynamic model of the atmosphere. J Atmos Sci 47: 2475–2487

Gibson JK, Kållberg P, Uppala S, Nomura A, Hernandez A, Serrano E, Gibson JK (1997) ERA description. In: ECMWF Re-Analysis Project Report Series, vol 1. ECMWF, Reading, UK

Hastenrath S (1979) Heat budget of tropical ocean and atmosphere. J Phys Oceanogr 10: 159–170

Houghton JT, Meira Filho LG, Callander BA, Harris N, Kattenberg A, Maskell K (eds) (1996) Climate change 1995, The science of climate change. Intergovernmental Panel on Climate Change, Cambridge University Press, Cambridge, UK

Kalnay E, Kanamitsu M, Kistler R, Deaven W, et al (1996) The NCEP/NCAR 40 year reanalysis project. Bull Am Meteorol Soc 77: 437–471

Kiehl JT, Trenberth KE (1997) Earth's annual global mean energy budget. Bull Am Meteorol Soc 78(2): 197–208

Lohmann G, Gerdes R, Chen D (1996) Sensitivity of the thermohaline circulation in coupled oceanic GCM – atmospheric EBM experiments. Clim Dyn 12: 403–416

Lorenz EN (1979) Forced and free variations of weather and climate. J Atmos Sci 36: 1367–1376

Manabe S, Stouffer RJ (1993) Century-scale effects of increased atmospheric CO_2 on the ocean-atmosphere system. Nature 364: 215–218

Masuda K (1988) Meridional heat transport by the atmosphere and the ocean: analysis of FGGE data. Tellus 40A: 285–302

Neeman BU, Ohring G, Joseph JH (1989) A parametrisation of eddy transfer coefficients for two-level seasonal statistical dynamical zonally averaged models. J Atmos Sci 46: 2371–2379

North GR, Mengel JG, Short DA (1983) Simple energy balance model resolving the seasons and the continents: application to the astronomical theory of ice ages. J Geophys Res 88(C11): 6576–6586

Oort AH (1971) The observed annual cycle in the meridional transport of atmospheric energy. J Atmos Sci 28: 325–339

Oort AH, Vonder Haar TH (1976) On the observed annual cycle in the ocean-atmosphere heat balance over the Northern Hemisphere. J Phys Oceanogr 6(6): 781–800

Schmittner A, Stocker TF (1999) The stability of the thermohaline circulation in global warming experiments. J Clim 12: 1117–1133

Sellers WD (1969) A global climate model based on the energy balance of the earth-atmosphere system. J Appl Meteorol 8: 1972–1983

Stendel M, Arpe K (1997) Evaluation of the hydrological cylce in reanalyses and observations. Max-Planck-Institut für Meteorologie, Hamburg, Germany, Tech Rep 228

Stocker TF, Schmittner A (1997) Influence of CO_2 emission rates on the stability of the thermohaline circulation. Nature 388: 862–865

Stocker TF, Wright DG, Mysak LA (1992) A zonally averaged, coupled ocean-atmosphere model for paleoclimate studies. J Clim 5: 773–797

Stone PH, Miller D (1980) Empirical relations between seasonal changes in meridional temperature gradients and meridional fluxes of heat. J Atmos Sci 37: 1708–1721

Stone PH, Yao M-S (1990) Development of a two-dimensional zonally averaged statistical-dynamical model. Part III: the parametrization of the eddy fluxes of heat and moisture. J Clim 3: 726–740

Wang Z, Mysak LA (1999) A simple coupled atmosphere-ocean-sea ice-land surface model for climate and paleoclimate studies. J Clim (in press)

Weaver AJ, Eby M, Fanning AF, Wiebe EC (1998) Simulated influence of carbon dioxide, orbital forcing and ice sheets of the climate of the Last Glacial Maximum. Nature 394: 847–853

Wild M, Ohmura A, Cubasch U (1997) GCM-simulated surface energy fluxes in climate change experiments. J Clim 10: 3093–3110